JOURNAL OF MECHANICAL ENGINEERING AND SCIENCES (JMES)
ISSN: 2289-4659 e-ISSN: 2231-8380
VOL. 15, ISSUE 2, 8016 – 8028
DOI: https://doi.org/10.15282/jmes.15.2.2021.07.0632

ORIGINAL ARTICLE

Numerical study of hemodynamics after stent implantation during the cardiac cycle

A. Belaghit[1], B. Aour[1], M. Larabi[2] , A. A. Tadjeddine[3], S. Mebarki[1]

[1] Laboratory of Applied Biomechanics and Biomaterials, Department of Mechanical Engineering, National Polytechnic School, Maurice Audin of Oran 31000, Algeria
Phone: +213(0)41582066
[2] Department of Mechanical Engineering, University of Sciences and Technology of Oran 31000, Algeria
[3] SCAMRE laboratory, Department of Electrical Engineering, National Polytechnic School, Maurice Audin of Oran 31000, Algeria

ABSTRACT – The descending aortic aneurysm is one of the most catastrophic cardiovascular emergencies resulting in high mortality worldwide. Clinical observations have pointed out that stent implantation in the sick aorta should probably allow stabilization of the hemodynamic state of the patient's aorta. To better understand the hemodynamic impact of a stent-treated aneurysm, numerical simulations are used to evaluate hemodynamic parameters. These latter including flow profile, velocity distribution, aortic wall pressure and shear stress, which are difficult to measure in vivo. It should be noted that the numerical modeling assists in medical planning by providing patterns of blood circulation, in particular, the distribution of pressures and shear stresses in the wall. In this context, the pulsatile blood flow in the aneurysmal aorta with stent is studied by CFD (Computational Fluid Dynamics) simulations. Realistic boundary conditions time dependent are prescribed at the level of the different arteries of the complete aorta models. The hemodynamic profile of the aneurysmal aorta with stent was analyzed by contour planes of velocity vectors, pressures and shear stresses at different times during the cardiac cycle. The obtained results made it possible to show the effect of the stent on the improvement of the blood flow by solving the problems of hemodynamic disturbances in the aorta. The methodology used in this work has revealed detailed and necessary information for the cases studied and shows the interest of the numerical tool for diagnosis and surgery.

ARTICLE HISTORY
Received: 03rd Apr 2020
Revised: 2nd June 2020
Accepted: 23rd Jan 2021

KEYWORDS
Blood flow;
pressure;
aorta;
stent;
systole;
diastole;
aneurysm

INTRODUCTION

Descending thoracic aortic aneurysms (DTAA) manifest as localized swelling of the descending aorta. They are difficult to detect because they usually have no symptoms. Without treatment, DTAA can eventually lead to rupture, ending by instant death[1, 2] The prevalence of aneurysmal disease in the elderly population is increasing, with around 150,000 new cases diagnosed each year [3].

Prevention of DTAA rupture is based on the treatment of open surgery. Endovascular aneurysm repair (EVAR) is an option currently available to treat DTAA [4]. In the EVAR procedure which has been developed in recent years, surgeons deploy a stent-graft (SG) through a small incision in the femoral artery to exclude aneurysms of the descending aorta, under the control of a live X-ray [5, 6].

Most current stent grafts use a combination of metal stents sewn to a polymeric fabric. EVAR has gained popularity because it reduces morbidity and postoperative mortality compared to open surgical procedures of the aorta [7]. However, to be successful, EVAR requires considerable surgeons experience due to non-intuitive visual perception via 2D projection from X-rays and of instruments indirect manipulation [8-10].

Traditional training methods, including the master-apprentice model and those using corpses, animals or plastic models, are often very expensive and have very limited value for personalized treatments [11, 12]. On the other hand, the numerical simulation of EVARs constitutes a versatile and cost-effective solution, which trainees can practice repeatedly in rare cases [13, 14]. In addition, patient-specific data can be quickly adopted to create a personalized virtual surgery environment for the planning of preoperative surgery, rehearsal, evaluation and optimization of interim surgical procedures, as well as better design of personalized stent grafts [15-18].

To achieve the complete structure of blood flow (vorticity, turbulence, pressure, shear stress, etc.), three-dimensional simulation techniques must be used, by working preferably on real arterial geometries, just like on real anatomies pathology obtained from MRI medical imaging [19]. In general, a CFD study makes it possible to obtain quantitative data of overall flow far from the wall or simply qualitative data [20, 21].

In this study, the hemodynamic effects of the pulsatile support mode on the aorta with stent were studied using the CFD method. A patient-specific aortic model, based on computed tomography data from a treated aneurysm patient (with stent), was reconstructed. The effects generated by the pulsatile support modes and wave of velocity and pressure were compared in order to clarify the different hemodynamic effects. The shear stresses applied to the wall were used as indicators to evaluate the hemodynamic states of the aorta with stent under different support modes, and on the

*CORRESPONDING AUTHOR | A. Belaghit | belaghithakim47@gmail.com

biomechanical environment of the pathological aorta with stent. All of this is established to assess the effectiveness of the stent and its effect on improving blood flow.

METHODS AND MATERIALS

The 3D reconstruction of the model studied is a fundamental phase of this numerical simulation. Figure 1 shows a CT scan imaging of the pathological aorta with stent of a 60-year-old man treated at the University Hospital of Oran (Algeria). Due to the complex geometry of the aorta, the procedure for obtaining the volume element personalized model from the biomedical images, we must go through several stages as shown in Figure 2 [21]. The first step is to recover the data from tomographic sections (CT-scan) which are performed in a repetitive manner with a regular interval of 0.5mm. The 3D geometry of the aorta model with stent was reconstructed from the DICOM (Digital Imaging and Communication in Medicine) format files of the CT scan image using Mimics software. Then, by a segmentation technique, we obtain the 3D geometrical model of the aorta which is numrically extracted in STL (stereolithography) format. The second step is carried out using the RapidForm software to obtain an ideal surface scan by correcting all geometrical faults and irregularities. The third step is to import data in IGES format of the aorta geometrical model in ANSYS-fluent software [22]. The model is discretized by finite volumes using 4-node tetrahedral elements (Figure 2).

Figure 1. MRI images for a 60-year-old man used to extract the geometry of aortic arch of the aorta with stent

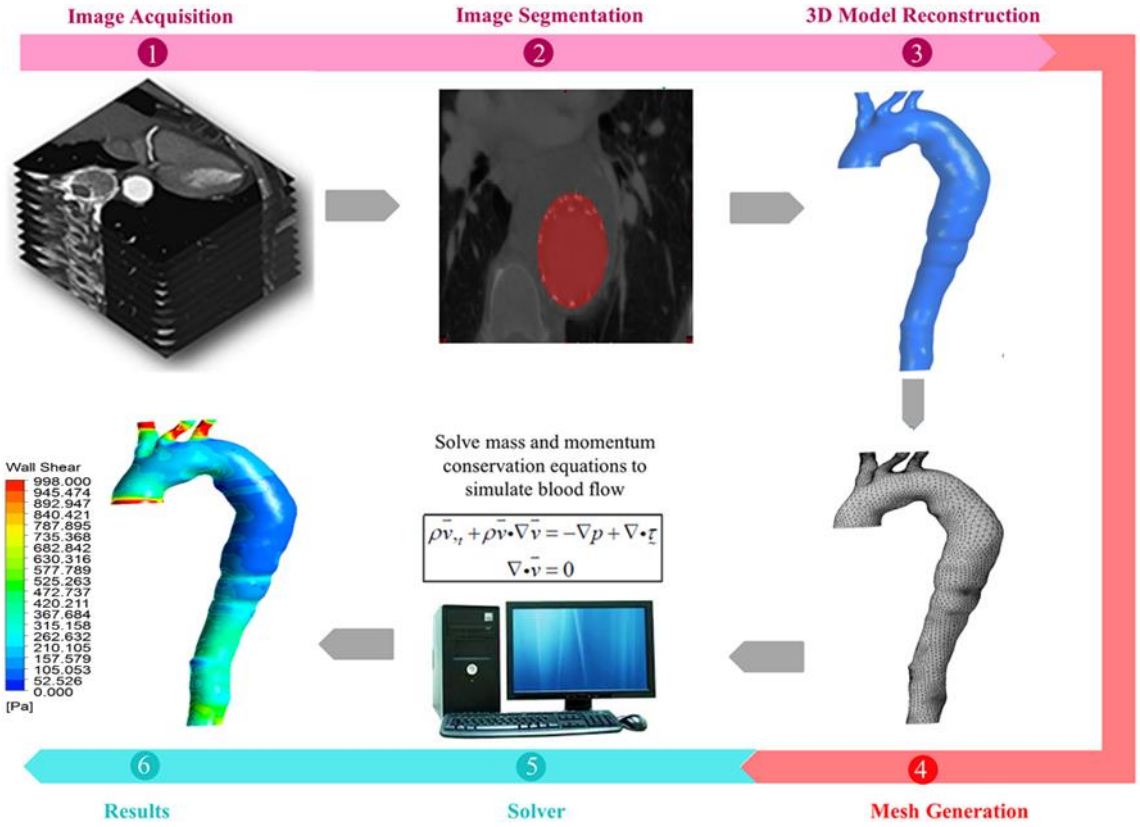

Figure 2. Procedure adopted for 3D reconstruction of the aorta model

NUMERICAL MODELING

Mathematical Model

The most widely used mathematical model for modeling flow phenomena is based on the resolution of Navier-Stokes partial differential equations (PDE) [23]. The arterial wall is assumed to be no-slip rigid. The blood is assumed to be incompressible. Therefore, a steady laminar blood flow can be described by the following Navier-Stokes equations:

$$\frac{\partial V}{\partial t} + (V.\nabla)V = -\frac{1}{\rho}\nabla p + \nu \nabla^2 V + f \tag{1}$$

$$\nabla.v = 0 \tag{2}$$

where V is the blood flow velocity vector, p denotes pressure, ρ represents blood density, ν is the kinematic viscosity and f represents the body force term per unit of mass.

These two equations are valid only when the fluid studied is Newtonian. Consecontly, they do not apply in all situations. They are used for example to model the whole blood in arteries [24] or only the plasma in the capillaries [25]. The presence of nonlinear terms in Navier-Stokes equations makes them difficult to solve analytically. It is therefore necessary to use numerical methods such as finite elements [26], finite volumes [27] or even finite differences [25] to find solutions. In this work, the finite volume method was used. Although, the use of such method requires precise conditioning of the problem in order to avoid the numerical instabilities due to the propagation of rounding errors, truncations or even discretization.

As simplifying assumptions, we consider blood as a homogeneous, incompressible, constant-density and viscous fluid. Moreover, the effect of gravity is neglected, and no thermal effects are considered. Vascular walls are modeled as non-permeable, rigid walls.

Boundary Conditions

The boundaries of the computational domain are usually represented by inlets, outlets, and walls. Inlets are often prescribed with velocity profile. A very common boundary condition is to use pressure on outlets. The boundary conditions for the arterial walls can be assumed rigid, have a prescribed motion, or deform as a consequence of the fluid pressure[28].

To study the pulsatile nature of blood flow, the velocity profile was defined at the aorta entrance. This velocity varies as a function of time and has been evaluated by experimental measurements [23]. The velocity wave at the entrance of the ascending aorta was estimated by Samuel and Fielden [29] using medical imaging (MRI) of 13 volunteers and a transit time technique. Figure 3(a) shows the representative velocity wave form, with a frequency of 1Hz and a maximum systolic velocity of 1.09 m/s. According to the literature, about 5% of blood flow the volume is outgoing to each of the three branches of the aorta. These outflows were assigned as velocity boundary conditions for the aortic arch branches. Zero-pressure boundary conditions were assigned at the three other outlets of the model, as shown in Figure 3(b). In this model, we assume the vessel walls are rigid with no-slip boundary conditions.

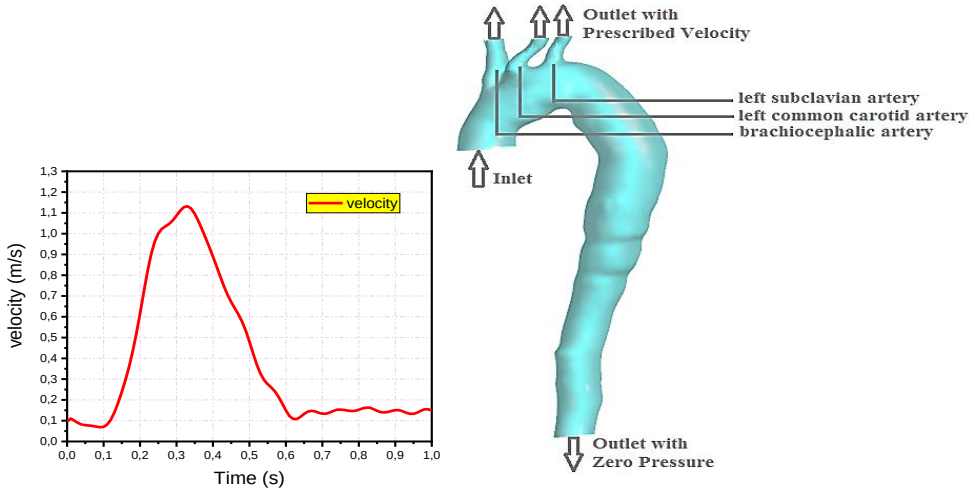

Figure 3. Illustration of the boundary conditions applied to the aorta: (a) profile of the transverse velocity at the entry of the ascending aorta, (according to [23]) and (b) boundary conditions at inlet and outlet

Regarding the blood flow in the large arteries, the shear rates in these latter are high enough which allow us to consider the flow passing through them as a Newtonian fluid, and incompressible [30]. The dynamic viscosity and the density of the blood are respectively 0.00371 Pa.s and 1060 kg/m^3 [31].

3D Finite Volume Modeling

In order to study the sensitivity of the mesh and choose the appropriate size, three types of meshes of the intact aorta with different numbers of elements were tested (see Table 1). The generation of the aorta model mesh was performed by ANSYS-Fluent code using 4-node linear tetrahedral elements. From the comparison between the results obtained for the maximum shear stresses using coarse, medium and fine meshes, it can be seen that there is a slight difference of 2.91% between the fine and medium meshes. Therefore, fine meshes of 864853 elements with 166131 nodes for aorta without stent (Figure 4(a)) and 9542150 elements with 176534 nodes for aorta with stent (Figure 4(b)) were selected for further analysis during this numerical investigation.

Table 1. Mesh sensitivity test results showing the maximum wall shear stresses values for different mesh element numbers of intact aorta model

Mesh type	Number of elements	Number of nodes	Max shear stress (Pa)	Difference (%)
Coarse	214195	48600	90	10
Medium	646590	127985	100	2.91
Fine	864853	166131	103	1.32

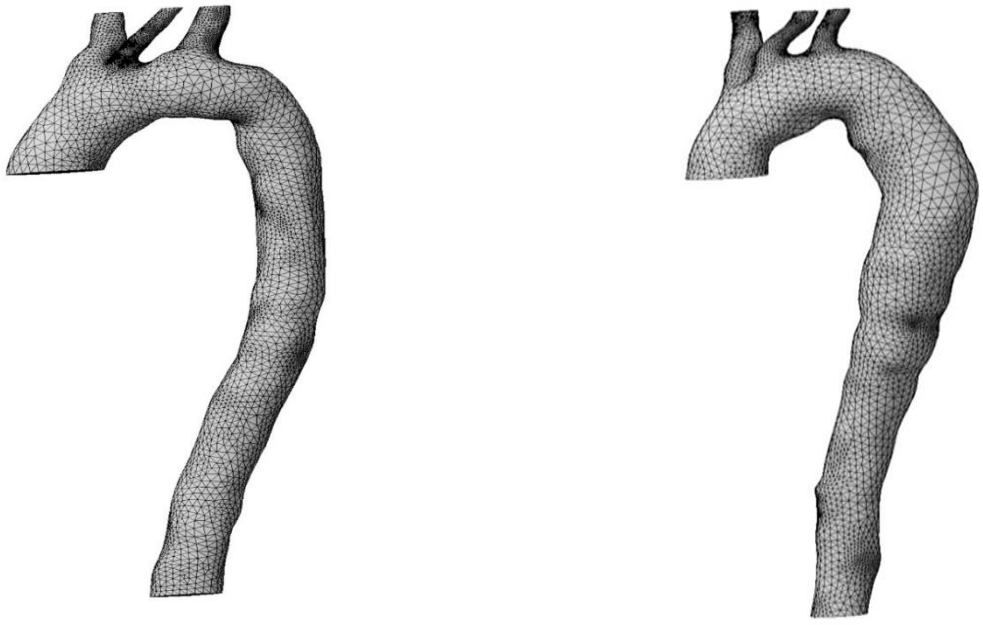

(a) (b)

Figure 4. Meshes used for the aortas models (a) without stent and (b) with stent

RESULTS AND DISCUSSION

The hemodynamic profile of the aneurysmal aorta with stent was analyzed by contour planes of velocity vectors, pressures and shear stresses at different times during the cardiac cycle. These six time instants represent the critical phases of flow in the cardiac cycle: t = 0.2 and 0.25s (maximum acceleration), t = 0.30s (maximum systole), 0.35s (maximum deceleration) and 0.4s (mid-diastole). Noting that these instants were chosen on the basis that each instant represents a critical time of the cardiac cycle [14, 32].

Stent Effect: Comparative Study

Figure 5 illustrates comparisons between the evolutions of the pressures (Figure 5(a)) and the velocities (Figure 5(b)) as a function of time in the case of an aneurysmal aorta with stent and the profile of an intact aorta, during the cardiac cycle. It can be seen that there are slight differences between both cases (with and without stent). Furthermore, a similar

behaviors have been noticed between both curves in the acceleration phase (between 0.15 and 0.25s). This confirms the effectiveness of the implanted stent and its effect on improving blood flow since both behaviors are almost similar.

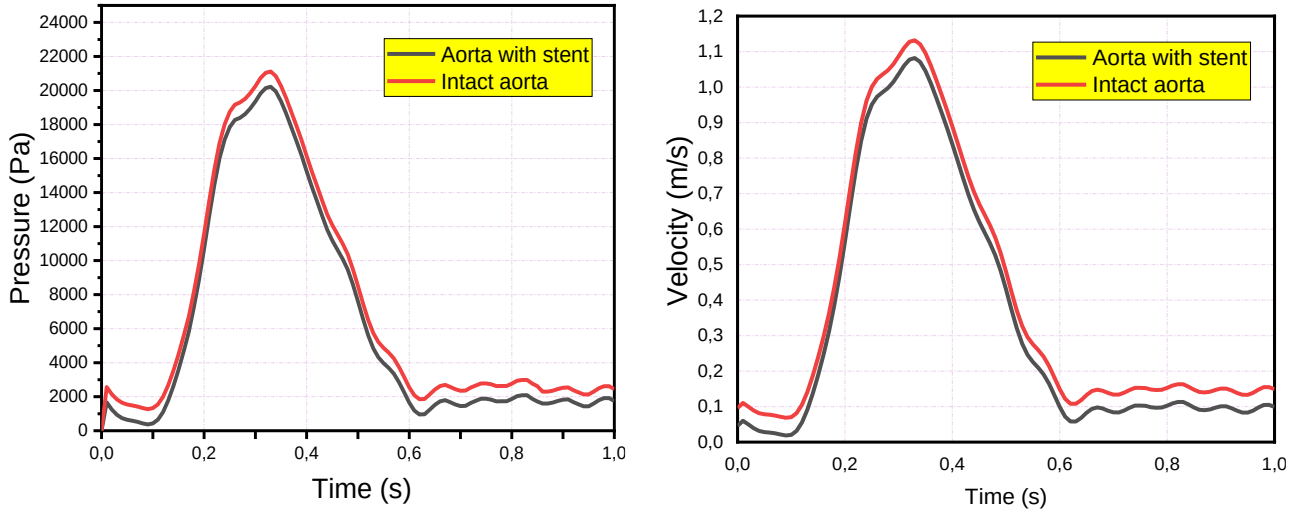

(a) (b)

Figure 5. Evolution of the pressures (a) and velocities and (b) as a function of time in the cases of an intact aorta and aorta with stent during the cardiac cycle

Distribution of Velocity Vectors

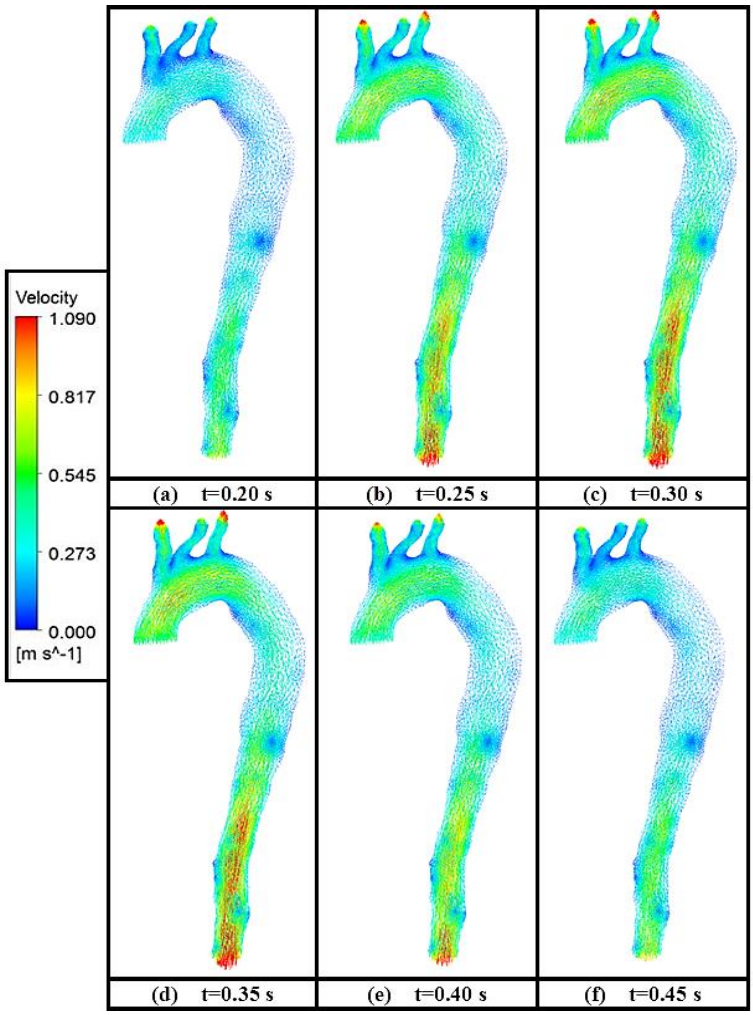

Figure 6. Distribution of velocity vectors in the aorta with stent at six consecutive critical moments of the cardiac cycle: (a-b) early systole (t = 0.20s), (t = 0.25s), (c-d) mid-systole (t = 0.3s) (t = 0.35s), (e) late systole (t = 0.4s) and (f) early diastole (t = 0.45s)

Figure 6 shows the velocity vectors of the aneurysmal aorta with stent at six instants of the cardiac cycle. The plot of the velocity vectors shows that the regions of high velocities are located at three positions : (i) the aortic arch, (ii) the branches of the distal part and (iii) the aorta outlet. The regions of low velocities appear in the ascending and descending aorta, when the vascular section is greater. The maximum value of velocity in the mid-systole phase (t = 0.3 and 0.35 s) increases slightly in the aorta model. The blood velocity then decreases at the end of systole (t = 0.40 s), and reaches its minimum value at the end of diastole (t = 0.45 s). This exhibits the effectiveness of the stent and its effect on improving blood flow since its behavior is almost similar to the normal state (Figure 5). In most moments of the cycle (t = 0s to 0.2s and 0.32 to 0.35s), a vortex appears at the end of the descending aorta just at the bottom region of the stent due to the sudden widening of the diameter (the fluid being released). The velocity of the vortex center is almost zero.

Distribution of Streamlines

The characteristic of the hemodynamic flow is captured by CFD simulations using the plotting of the aortic input streamlines at different times of the cardiac cycle. Figure 7 shows the streamlines of the aneurysmal aorta with stent. It can be noted that the blood flow is relatively low at the start of systole (t = 0.20 and 0.25s). The initiation of flow occurs in the proximal ascending aorta, only in the middle systole (t = 0.3s) when the velocities are highest. The flow reaches its maximum intensity when the vascular section is smaller at the level of the proximal ascending aorta and at the end of the aorta. The blood flow then decreases during late systole (t = 0.40 s).

During the systolic acceleration phase, the streamlines in the stent zone are mainly parallel to the aortic wall, in particular, in the proximal region. This highlighted the effectiveness of the stent type chosen and its effect on improving the blood flow.

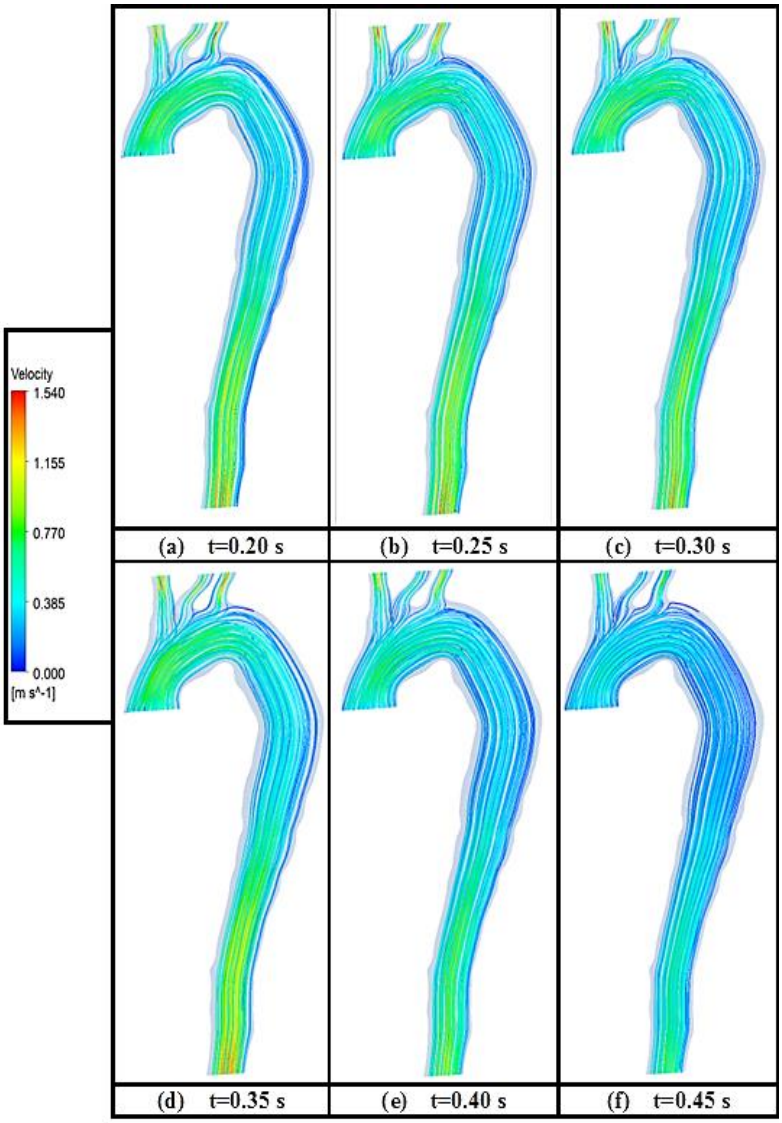

Figure 7. Illustration of the aorta streamlines at six consecutive critical moments of the cardiac cycle: (a-b) early systole (t = 0.20s), (t = 0.25s), (c-d) mid-systole (t = 0.3 s) (t = 0.35s), (e) late systole (t = 0.4 s) and (f) early diastole (t = 0.45s)

Figure 8 shows the evolution of the velocity at the entrance (Plane 1), in the region of the aortic arch (Plane 2), in the region of the aneurysmal sac with stent (Planes 3 and 4), and in the inferior region of the descending aorta (Plane 5). Qualitatively, we note that the simulations of the blood flow reproduce certain transitory flow characteristics, mainly the phase delay (Planes 3 and 4) of the peak systole compared to the waveform of the input flow (Plane 1). This is due to the change in the aorta section.

Nevertheless, we have shown the effect of aortic wave reflections on the flow profiles obtained in several planes of the aortic model with stent. The delay in systolic flow and its reduction when the velocity wave crosses the pathological aorta with stent is justified by the complex flow in the branches of the aorta which may explain the differences observed in the flow waveforms at the entrance and at the middle of the section. It can be also observed that there is a slight difference between the velocity variations in planes 3 and 4, which comfirms the good choice of the stent and its effect on improving the blood flow in the aorta.

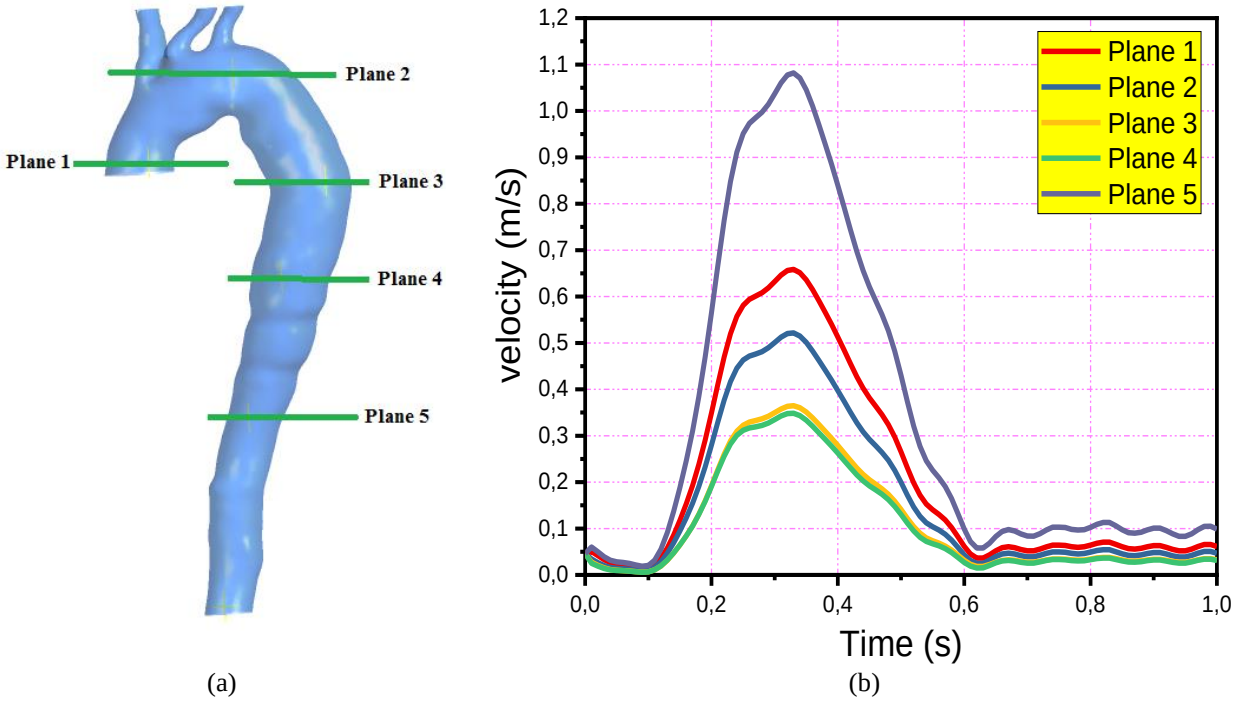

(a) (b)

Figure 8. Evolution of the velocity at the entrance (Plane 1), in the region of the aortic arch (Plane 2), in the region of the aneurysmal sac with stent (Planes 3 and 4), and in the lower region of the descending aorta (Plane 5)

An interesting aspect of the 3D flows analysis in the cardiovascular system is the graphic presentation of the flow field. Figures 9, 10 and 11 show contours plots of the velocity amplitude in the aortic arch for three different moments: maximum systole (t = 0.33s: which is the time at which the pressure gradient between the ascending and descending aorta becomes maximal), a point near the end of the systole (t = 0.4 s) and at the early diastole (t = 0.45 s).

The results show that the time points with a maximum input velocity are at t = 0.33s (Figure 9, maximum systole). The flow at the ascending aorta (plane 1) is systematically oriented towards the internal aortic wall. This vortex type velocity profile was induced by the geometry of the curved entry and does not result from the boundary conditions at the inlet. In the descending aorta (plane 3), the maximum velocity decreases from 1 m/s to 0.7 m/s due to the growth of the diameter. In plane 4, there is a slight increase in velocity at the axis of the aorta. The velocity reaches its maximum value in plane 5 with resemblance to the regular flow. Due to the non-planar anatomy of the aorta, the flow is strongly inclined towards the anterior wall of the aorta, then it incline towards the external wall (see Figure 9). Furthermore, during the (diastolic) deceleration phase at t = 0.4s (Figure 10), the flow patterns are similar to those observed at the systolic peak, with a regular decrease in velocity.

On the other hand, Figure 11 shows the contours of the primary velocity in the cross sections of the aorta model at the minimum inlet velocity (t = 0.45s). The velocity contour plots in the aortic arch and branches are generally symmetrical, with a slightly asymmetrical profile. A significant decrease in the velocity field was observed, compared to the previous cases. Most of these flow characteristics are due to the lower velocities and Reynolds numbers that occur during the minimum flow.

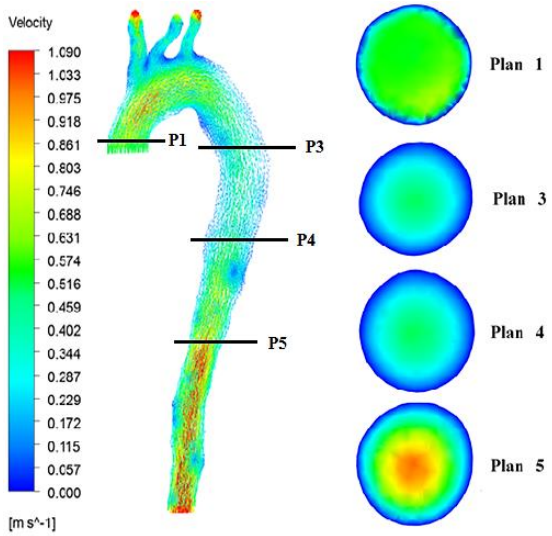

Figure 9. Velocity contour plots at different cross sections along the aorta at t = 0.33s

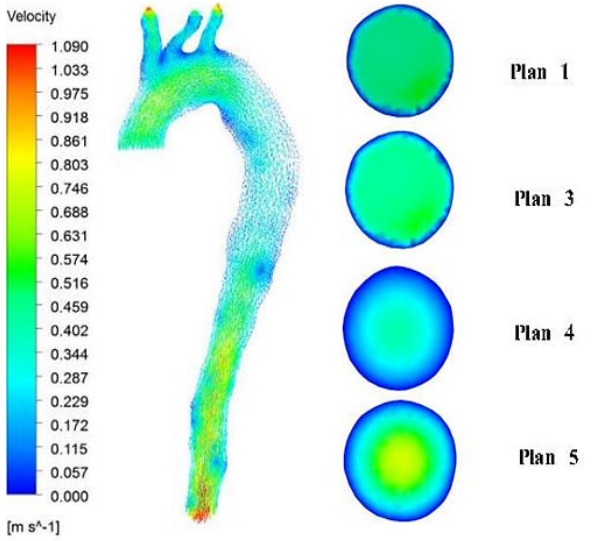

Figure 10. Velocity contour plots different cross sections along the aorta at t = 0.4s

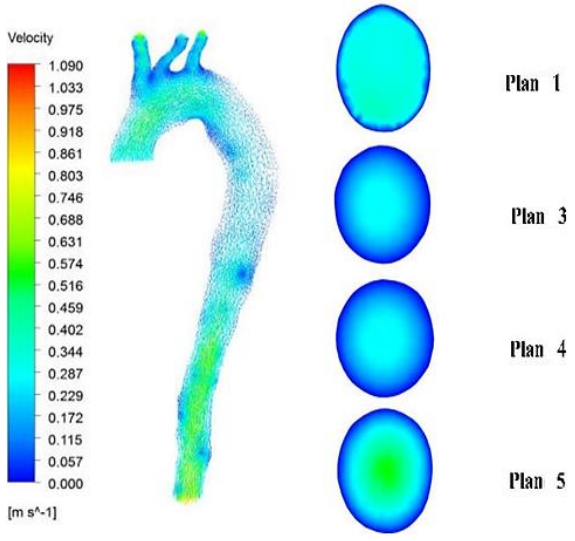

Figure 11. Velocity contour plots at different cross sections along the aorta at t = 0.45s

Pressure Distribution

The pressure contours throughout the cardiac cycle are shown in Figure 12. The pressure gradient generally decreases in the flow direction along the aorta. The highest pressure is approximately 19.13 kPa (150.99 mm Hg) and is localized at the aortic root and at the ascending aorta. The region of low pressure is located in the iliac arteries due to the coarctation of these latter. This pressure is similar to the outlet pressure of 15.68 kPa (117.61 mm Hg) at maximum systole. When the vascular section is larger, the pressure value decreases. The pressure increases slightly in the aorta model at maximum systole (t = 0.3 and 0.35 s). The blood pressure then decreases in the late systole with a regular decrease (t = 0.40 s), and reaches its minimum value at the end of the diastole (t = 0.45 s).

The results obtained within the framework of this study made it possible to evaluate the implantation effect of the stent. It has been found that the stent makes the flow more linear and structured in the aneurysm region, while stabilizing the pressures. The results thus presented showed that the stent could limit the dilation of the descending aorta. This also confirms the effectiveness of the stent type used and its effect on improving blood flow.

The laminar nature of the flow field is highlighted in Figure 13, where we show the temporal evolutions of the pressure amplitude in five transverse planes of the pathological aorta axis with stent. It is clear that no pressure oscillation is present during the whole cardiac cycle. In addition, a pressure difference between the different planes with respect to the aorta inlet (Plane 1) during the systolic phase has been observed. This is due to the complex geometry of the aorta (narrowing, high curvature) and the presence of the branches, which generates, consequently, a complex flow in the aorta. Indeed, these parameters seem to be crucial factors justifying the pressures differences between the planes.

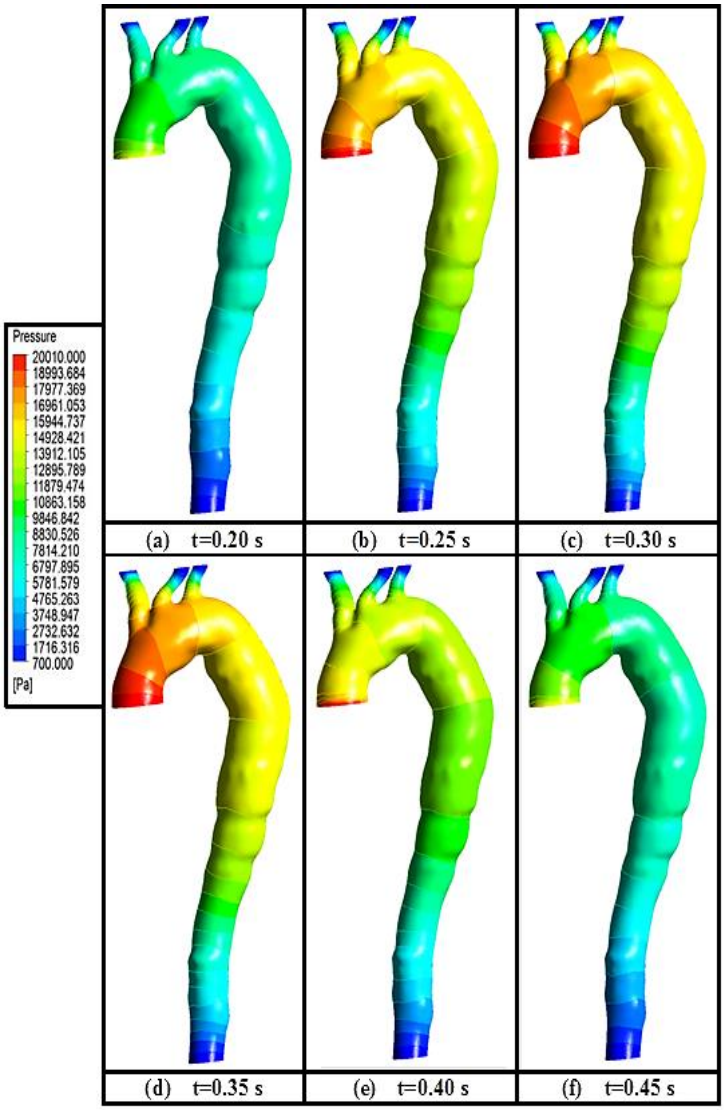

Figure 12. Pressure distribution in the aorta at six consecutive critical moments of the cardiac cycle: (a-b) early systole (t = 0.20 and 0.25 s), (c-d) mid-systole (t = 0.3 and 0.35 s), (e) late systole (t = 0.4 s) and (f) early diastole (t = 0.45 s)

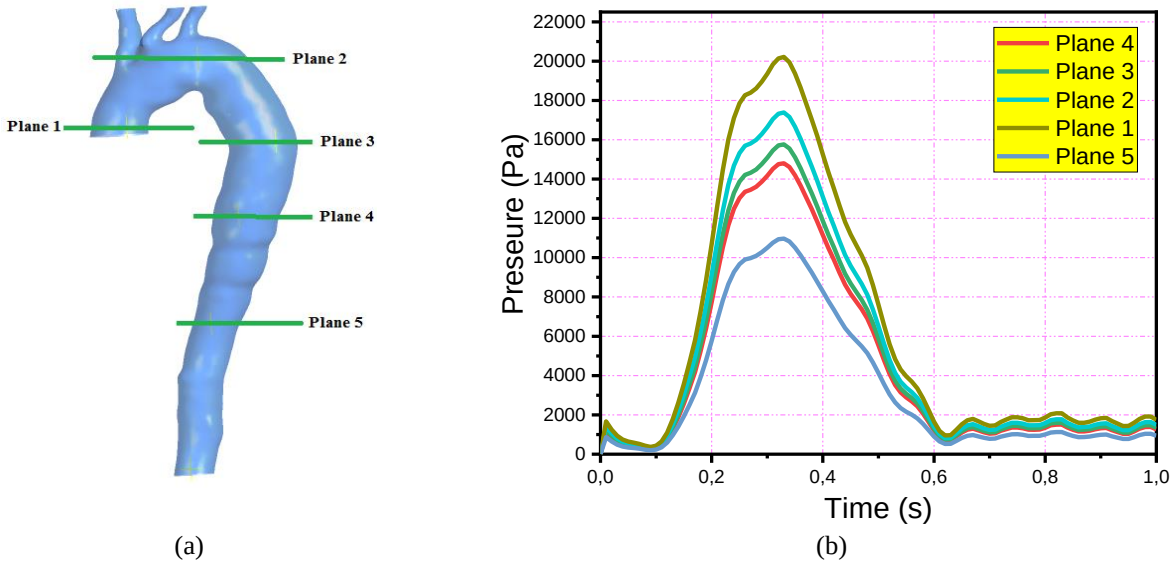

(a) (b)

Figure 13. Evolution of the pressure at the inlet (Plane 1), in the region of the aortic arch (Plane 2), in the region of the aneurysmal sac with stent (Planes 3 and 4), and in the lower region of the descending aorta (Plane 5)

Distribution of Shear Stresses

Figure 14 illustrates the distribution of shear stresses in the aorta with stent throughout the cardiac cycle. The contour plots are shown for (a-b) early systole (t = 0.20 and 0.25 s); (c-d) mid-systole (t = 0.3 and 0.35 s); (e) late systole (t = 0.4 s) and (f) early diastole (t = 0.45 s). It should be noted that the area of high shear stresses is observed in the proximal ascending aorta (near the aortic entrance). Throughout the cardiac cycle, it can be seen that the distribution of shear stresses is strongly correlated with the previous results of the flow streamlines and the velocity fields. In the systolic acceleration phase (t = 0.20 and 0.25s), the pathological aorta with stent has a relatively moderate distribution of shear stresses in the section of the proximal ascending aorta. Then, it becomes asymmetric , due to the curvature of the wall and the subsequent flow towards the internal wall. An area of high shear stresses appears at the beginning of the interior curvature of the ascending aorta. Low values of shear stresses are presented on the outer wall, then they increase slightly as the blood moves through the distal ascending aorta.

At maximum systole (t = 0.3 and 0.35s) and due to the high blood velocities observed for this cardiac instant, the shear stresses increase significantly along the aorta, as shown in Figure 14. The distribution of shear stresses at this cardiac moment follows the trend initiated in the acceleration phase, where the values of the highest shear stresses are observed in the internal curvature of the ascending aorta and are around 28Pa.

As the velocities of the blood flow decrease slightly in the aortic arch and at the level of the inlets of the supra-aortic arteries, the shear stresses in these zones are lower. Maximum values of shear stresses are observed, in correlation with the high velocities observed in these regions. Shear stresses also increase in the proximal descending aorta in maximum systole (t = 0.3 and 0.35s) compared to systolic acceleration (t = 0.20 and 0.25s). They follow the trend of blood flow, as shown in Figure 14. Furthermore, we note systolic shear stresses more prononced at the external curvature of the ascending aortic wall, which are in agreement with the results of the literature [33, 34].

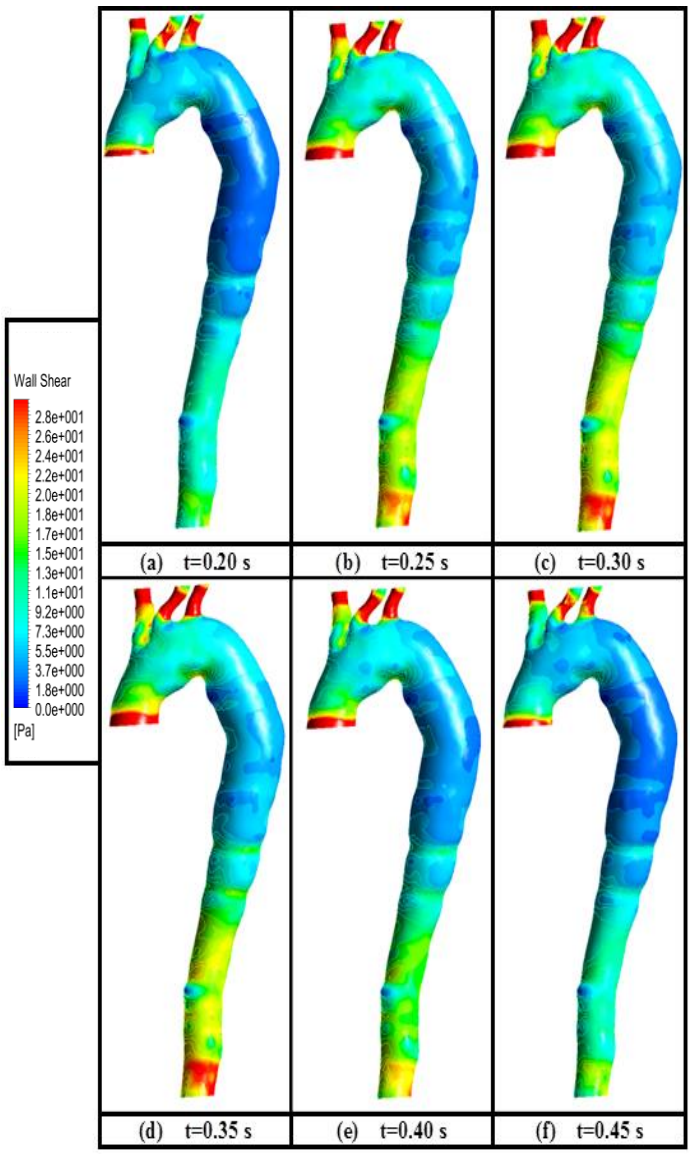

Figure 14. Distribution of shear stresses of the aorta at six consecutive critical moments in the cardiac cycle: (a-b) early systole (t = 0.20 and 0.25s), (c-d) midi-systole (t = 0.3 and 0.35s), (e) late systole (t = 0.4s) and (f) early diastole (t = 0.45s)

CONCLUSIONS

The results obtained within the framework of this study made it possible to evaluate the effect of the stent implantation during the consecutive critical moments of the cardiac cycle. CFD simulations have shown that stent deployment tends to normalize flow structures in the pathological aorta. Indeed, we have found that the stent makes the flow more linear and structured in the aneurysm area, while limiting turbulence and stabilizing the flow velocities and the pressures and reducing the shear stresses in the walls of the aorta. The results thus presented showed that the stent could limit the dilation of the descending aorta, which confirms the effectiveness of the stent type used and its effect on improving blood flow. Finally, it is interesting to note that the models developed within the framework of this present work could be essential help tools for vascular surgery during pre- and post-surgical intervention in order to make the adequate decisions and to evaluate the results of the surgical intervention.

ACKNOWLEDGMENTS

The authors would like to acknowledge the General Directorate of Scientific Research and Technological Development (DGRSDT), Ministry of Higher Education and Scientific Research of Algeria and LABAB Laboratory of National Polytechnic School of Oran for research grants and funding.

REFERENCES

[1] G. Johansson and J. Swedenborg, "Ruptured abdominal aortic aneurysms: A study of incidence and mortality," *British Journal of Surgery*, vol. 73, no. 2, pp. 101-103, 1986. doi: 10.1002/bjs.1800730205.

[2] E. K. Shang *et al.*, "Impact of Wall Thickness and Saccular Geometry on the Computational Wall Stress of Descending Thoracic Aortic Aneurysms," vol. 128, no. 11_suppl_1, pp. S157-S162, 2013.

[3] N. Kontopodis, S. Lioudaki, D. Pantidis, G. Papadopoulos, E. Georgakarakos, and C. V. Ioannou, "Advances in determining abdominal aortic aneurysm size and growth," (in eng), *World J Radiol*, vol. 8, no. 2, pp. 148-58, Feb 28 2016. doi: 10.4329/wjr.v8.i2.148.

[4] R. M. Greenhalgh, L. C. Brown, G. P. Kwong, J. T. Powell, and S. G. Thompson, "Comparison of endovascular aneurysm repair with open repair in patients with abdominal aortic aneurysm (EVAR trial 1), 30-day operative mortality results: randomised controlled trial," (in eng), *Lancet*, vol. 364, no. 9437, pp. 843-8, Sep 4-10 2004. doi: 10.1016/s0140-6736(04)16979-1.

[5] R. S. Jackson, D. C. Chang, and J. A. Freischlag, "Comparison of long-term survival after open vs endovascular repair of intact abdominal aortic aneurysm among Medicare beneficiaries," (in eng), *Jama*, vol. 307, no. 15, pp. 1621-8, Apr 18 2012. doi: 10.1001/jama.2012.453.

[6] M. Prinssen *et al.*, "A randomized trial comparing conventional and endovascular repair of abdominal aortic aneurysms," (in eng), *N Engl J Med*, vol. 351, no. 16, pp. 1607-18, Oct 14 2004. doi: 10.1056/NEJMoa042002.

[7] Y. Bryce, P. Rogoff, D. Romanelli, and R. Reichle, "Endovascular repair of abdominal aortic aneurysms: vascular anatomy, device selection, procedure, and procedure-specific complications," (in eng), *Radiographics*, vol. 35, no. 2, pp. 593-615, Mar-Apr 2015. doi: 10.1148/rg.352140045.

[8] R. J. Hinchliffe, L. Bruijstens, S. T. MacSweeney, and B. D. Braithwaite, "A randomised trial of endovascular and open surgery for ruptured abdominal aortic aneurysm - results of a pilot study and lessons learned for future studies," (in eng), *Eur J Vasc Endovasc Surg*, vol. 32, no. 5, pp. 506-13; discussion 514-5, Nov 2006. doi: 10.1016/j.ejvs.2006.05.016.

[9] P. Desgranges, H. Kobeiter, Y. Castier, M. Sénéchal, M. Majewski, and A. Krimi, "The Endovasculaire vs Chirurgie dans les Anévrysmes Rompus Protocol trial update," (in eng), *J Vasc Surg*, vol. 51, no. 1, pp. 267-70, Jan 2010. doi: 10.1016/j.jvs.2009.10.128.

[10] G. H. White, W. Yu, and J. May, "Endoleak--a proposed new terminology to describe incomplete aneurysm exclusion by an endoluminal graft," (in eng), *J Endovasc Surg*, vol. 3, no. 1, pp. 124-5, Feb 1996. doi: 10.1583/1074-6218(1996)003<0124b:>2.0.CO;2.

[11] D. D. Mendoza *et al.*, "Impact of image analysis methodology on diagnostic and surgical classification of patients with thoracic aortic aneurysms," (in eng), *Ann Thorac Surg*, vol. 92, no. 3, pp. 904-12, Sep 2011. doi: 10.1016/j.athoracsur.2011.03.130.

[12] L. E. Quint, P. S. Liu, A. M. Booher, K. Watcharotone, and J. D. Myles, "Proximal thoracic aortic diameter measurements at CT: repeatability and reproducibility according to measurement method," (in eng), *Int J Cardiovasc Imaging*, vol. 29, no. 2, pp. 479-88, Feb 2013. doi: 10.1007/s10554-012-0102-9.

[13] U. Morbiducci *et al.*, "In vivo quantification of helical blood flow in human aorta by time-resolved three-dimensional cine phase contrast magnetic resonance imaging," (in eng), *Ann Biomed Eng*, vol. 37, no. 3, pp. 516-31, Mar 2009. doi: 10.1007/s10439-008-9609-6.

[14] K. M. Tse, P. Chiu, H. P. Lee, and P. Ho, "Investigation of hemodynamics in the development of dissecting aneurysm within patient-specific dissecting aneurismal aortas using computational fluid dynamics (CFD) simulations," (in eng), *J Biomech*, vol. 44, no. 5, pp. 827-36, Mar 15 2011. doi: 10.1016/j.jbiomech.2010.12.014.

[15] A. Caballero, S. J. C. E. Laín, and Technology, "A review on computational fluid dynamics modelling in human thoracic aorta," vol. 4, pp. 103-130, 2013.

[16] U. Morbiducci *et al.*, "Outflow conditions for image-based hemodynamic models of the carotid bifurcation: implications for indicators of abnormal flow," (in eng), *J Biomech Eng*, vol. 132, no. 9, p. 091005, Sep 2010. doi: 10.1115/1.4001886.

[17] U. Morbiducci, R. Ponzini, D. Gallo, C. Bignardi, and G. Rizzo, "Inflow boundary conditions for image-based computational hemodynamics: impact of idealized versus measured velocity profiles in the human aorta," (in eng), *J Biomech*, vol. 46, no. 1, pp. 102-9, Jan 4 2013. doi: 10.1016/j.jbiomech.2012.10.012.

[18] I. C. Campbell, J. Ries, S. S. Dhawan, A. A. Quyyumi, W. R. Taylor, and J. N. Oshinski, "Effect of inlet velocity profiles on patient-specific computational fluid dynamics simulations of the carotid bifurcation," (in eng), *J Biomech Eng*, vol. 134, no. 5, p. 051001, May 2012. doi: 10.1115/1.4006681.

[19] C. A. T. and and M. T. Draney, "Experimental and computational methods in cardiovascular fluid mechanics," vol. 36, no. 1, pp. 197-231, 2004. doi: 10.1146/annurev.fluid.36.050802.121944.

[20] J. Lantz, J. Renner, and M. Karlsson, "Wall shear stress in a subject specific human aorta — influence of fluid-structure interaction," vol. 03, no. 04, pp. 759-778, 2011. doi: 10.1142/s1758825111001226.

[21] A. Belaghit, B. Aour, M. Larabi, S. J. J. o. B. Mebarki, Biomaterials, and B. Engineering, "Numerical modeling of blood flow in a healthy aorta and aorta with stent," vol. 39, pp. 13 - 23, 2018.

[22] X. Zhang *et al.*, "Analysis of the formation mechanism and occurrence possibility of Post-Stenotic Dilatation of the aorta by CFD approach," *Computer Methods and Programs in Biomedicine*, vol. 194, p. 105522, 2020/10/01/ 2020. doi: https://doi.org/10.1016/j.cmpb.2020.105522.

[23] T. Petrila and D. Trif, *Basics of Fluid Mechanics and Introduction to Computational Fluid Dynamics*, 1 ed. (Numerical Methods and Algorithms, no. 3). Springer US, 2005, pp. XIV, 500.

[24] T. Bodnár and A. Sequeira, "Numerical Simulation of the Coagulation Dynamics of Blood," *Computational and Mathematical Methods in Medicine*, vol. 9, p. 143803, 1900/01/01 2008. doi: 10.1080/17486700701852784.

[25] P. Bagchi, "Mesoscale simulation of blood flow in small vessels," (in eng), *Biophys J*, vol. 92, no. 6, pp. 1858-77, Mar 15 2007. doi: 10.1529/biophysj.106.095042.

[26] M. C. Arokiaraj, M. De Beule, and G. De Santis, "A novel sax-stent method in treatment of ascending aorta and aortic arch aneurysms evaluated by finite element simulations," (in eng), *J Med Vasc*, vol. 42, no. 1, pp. 39-45, Feb 2017. doi: 10.1016/j.jdmv.2017.01.005.

[27] A. Caimi *et al.*, "Prediction of post-stenting biomechanics in coarcted aortas: A pilot finite element study," *Journal of Biomechanics*, vol. 105, p. 109796, 2020/05/22/ 2020. doi: https://doi.org/10.1016/j.jbiomech.2020.109796.

[28] J. Lantz, "On Aortic Blood Flow Simulations Scale-Resolved Image-Based CFD," Department of Management and Engineering, Applied Thermodynamics and Fluid Mechanics, Dissertation Linköping University, Sweden, 2013.

[29] S. W. Fielden, B. K. Fornwalt, M. Jerosch-Herold, R. L. Eisner, A. E. Stillman, and J. N. Oshinski, "A new method for the determination of aortic pulse wave velocity using cross-correlation on 2D PCMR velocity data," (in eng), *J Magn Reson Imaging*, vol. 27, no. 6, pp. 1382-7, Jun 2008. doi: 10.1002/jmri.21387.

[30] M. S. Olufsen, C. S. Peskin, W. Y. Kim, E. M. Pedersen, A. Nadim, and J. Larsen, "Numerical simulation and experimental validation of blood flow in arteries with structured-tree outflow conditions," (in eng), *Ann Biomed Eng*, vol. 28, no. 11, pp. 1281-99, Nov-Dec 2000. doi: 10.1114/1.1326031.

[31] P. B. Dobrin, "Mechanics of normal and diseased blood vessels," (in eng), *Ann Vasc Surg*, vol. 2, no. 3, pp. 283-94, Jul 1988. doi: 10.1016/s0890-5096(07)60016-8.

[32] S. Chandra *et al.*, "Fluid-structure interaction modeling of abdominal aortic aneurysms: the impact of patient-specific inflow conditions and fluid/solid coupling," (in eng), *J Biomech Eng*, vol. 135, no. 8, p. 81001, Aug 2013. doi: 10.1115/1.4024275.

[33] T. A. Chuter *et al.*, "Endoleak after endovascular repair of abdominal aortic aneurysm," (in eng), *J Vasc Surg*, vol. 34, no. 1, pp. 98-105, Jul 2001. doi: 10.1067/mva.2001.111487.

[34] R. B. Rutherford and W. C. Krupski, "Current status of open versus endovascular stent-graft repair of abdominal aortic aneurysm," (in eng), *J Vasc Surg*, vol. 39, no. 5, pp. 1129-39, May 2004. doi: 10.1016/j.jvs.2004.02.027.